19. J. Gauthier, A. G. Kluge, T. Rowe, *Cladistics* **4**, 105 (1988).
20. D. M. Irwin and A. C. Wilson, in (*2*), pp. 257–267.
21. J. A. Lillegraven, S. D. Thompson, B. K. McNab, J. L. Patton, *Biol. J. Linnean Soc.* **32**, 281 (1987); M. B. Renfree, in *Mesozoic Differentiation; Multituberculates, Monotremes, Early Therians, and Marsupials*, vol. 1 of *Mammal Phylogeny*, F. S. Szalay, M. J. Novacek, M. C. McKenna, Eds. (Springer-Verlag, New York, 1993), pp. 4–20.
22. All terminal taxa except the hypothetical ancestor were run as a single polytomy in order to assess the monophyly of Ungulatomorpha. In Table 1, all multistate characters were run unordered; all numbered states followed by a question mark were run as the state indicated; those given only as a question mark were run as missing data. The default settings of the branch-and-bound method of PAUP [D. L. Swofford, *PAUP: Phylogenetic Analysis Using Parsimony, Version 3.1* (Illinois Natural History Survey, Champaign, IL, 1993)] were used. The results were four equally parsimonious trees with a tree length of 67 steps, in which only the position of the various nonungulatomorphs changed, thus the strict consensus tree in Fig. 1. The measures for each tree were as follows: (i) consistency index = 0.701; (ii) homoplasy index = 0.582; (iii) retention index = 0.773; and (iv) rescaled consistency index = 0.542. I ran a second analysis, using the heuristic method to determine the shortest tree, that did not hold Ungulatomorpha as monophyletic. The run yielded 2047 equally parsimonious trees, each of 69 steps. The measures for each of these trees were as follows: (i) consistency index = 0.681; (ii) homoplasy index = 0.594; (iii) retention index = 0.750; and (iv) rescaled consistency index = 0.511.
23. P. D. Gingerich, D. P. Domning, C. E. Blane, M. D. Uhen, *Contrib. Mus. Paleontol. Univ. Mich.* **29**, 41 (1994).
24. Upper dentition characters and character states for taxa shown in Table 1 and used in the phylogenetic analysis in Fig. 1 are as follows: Primitive or ancestral state = 0, derived = 1 to 3, and missing = ?. *Metaconule reduced. **Usually only four premolars at most. †Has only three premolars. Characters are as follows: (a) Amount of anteroposterior expansion of protocone: none (0), slight (1), moderate (2), substantial (3). (b) Amount of labial shift of protocone: none (0), moderate (1), substantial (2). (c) Postparaconular and premetaconular cristae: strong and winglike (0), weak or absent (1). (d) Metacingulum: formed only of the postmetaconule crista and terminates dorsal of postmetacrista, which is continuous with the metastylar lobe (0), formed of the postmetaconule crista continuing on to the metastylar lobe (1). (e) Stylar shelf: wide (0), narrow (1). (f) Number of cuspules in parastylar region: one (0), two (1). (g) Pre- and postcingula: do not have or have only a hint of cingula (0), cingula do not reach or extend below the conules (1), cingula reach or extend below the conules (2). (h) Height and size of para- and metacone: paracone higher and larger (0), cusps of similar height and size (1). (i) Metacone or metaconal swelling on P^5 (or ultimate upper premolar): absent (0), present (1). (j) Number of premolars: five (0), four or fewer (1). (k) Shape of molar crown in occlusal view: triangular (0), trapezoidal (1), subrectangular (2), rectangular (3). (l) Constriction of crown through conular region without or without cingula present: no constriction and no cingula (0); marked constriction and with cingula (1), slight constriction and with cingula (2), no constriction with cingula (3). (m) Ectoflexus: deep (0), shallow (1), none (2). (n) M^3 linguolabial width relative to other molars: not markedly narrowed (0), markedly narrowed (1). (o) Parastylar groove: well developed (0), very reduced or absent (1). (p) Base of paracone and metacone: merged (0), separate (1). (q) Distance between paracone or metacone and protocone relative to total anterior or posterior width, respectively: between 45 and 55% of crown width (0), more than 55% of crown width (1), less than 45% of crown width (2). (r) Position of conules (especially paraconule) relative to paracone and metacone versus protocone: conules closer to mid-position (0), conules closer to protocone than to the mid-position (1).
25. Z. Kielan-Jaworowska, T. M. Bown, J. A. Lillegraven, in *Mesozoic Mammals: The First Two-Thirds of Mammalian History*, J. A. Lillegraven, Z. Kielan-Jaworowska, W. A. Clemens, Eds. (Univ. of California Press, Berkeley, 1978), pp. 99–149.
26. L. A. Nessov, *Tr. Zool. Inst. Ross Akad. Nauk SSSR* **249**, 105 (1993).
27. R. L. Carroll, *Vertebrate Paleontology and Evolution* (Freeman, New York, 1988).
28. I thank L. A. Nessov, O. I. Tsaruk, and B. G. Veretennikov for help in the field; D. A. Azimov and O. I. Tsaruk for logistical support while in Uzbekistan for the 1994 field season; A. Berta, R. Etheridge, Z. Kielan-Jaworowska, and J. A. Lillegraven for helpful comments; J. H. Hutchison, R. C. Fox, W. A. Clemens, and R. L. Cifelli for casts or the loan of material; and L. A. Nessov and Z. Kielan-Jaworowska for photographs in Fig. 2, A through D, G, and F. I am especially grateful to the late L. A. Nessov, without whose pioneering fieldwork and earlier studies, this analysis would not have been possible. The 1994 field season and preparation of this manuscript were supported by the National Geographic Society (L. A. Nessov and J.D.A.).

13 February 1996; accepted 25 March 1996

Bacteria as Mediators of Copper Sulfide Enrichment During Weathering

Richard H. Sillitoe,* Robert L. Folk, Nicolás Saric

Supergene chalcocite enrichment during weathering is an economically vital natural process that may lead to severalfold increases in the copper content of sulfide deposits. A scanning electron microscope study of chalcocite (Cu_2S) from major enriched copper deposits in northern Chile revealed myriad bacterioform bodies in original growth positions near replacement interfaces with remnant hypogene sulfide grains. These minute (0.03 to 0.2 micrometers) chalcocite bodies are interpreted as fossilized and metallized nannobacteria that promoted the fixation of mobilized copper ions. Bacterial activity may thus be a fundamental factor in supergene enrichment of copper deposits.

Many of the world's major Cu deposits were formed by supergene enrichment during weathering. Enrichment took place at and beneath the ground-water table under reducing conditions and involved the progressive replacement of hypogene sulfides, especially chalcopyrite ($CuFeS_2$) and pyrite, by Cu-rich sulfides of the chalcocite (Cu_2S) group (*1*–*3*). The necessary Cu, supplied by descending acidic solutions at ambient temperatures, was obtained by oxidative dissolution of cupriferous sulfides in the vadose zone above the ground-water table (Fig. 1). Sulfide oxidation is promoted by acidophilic bacteria, both in the natural environment and in commercial beneficiation of chalcocite and other ores (*4*, *5*), but Cu enrichment typically has been modeled as an abiotic process. Here we present results from a scanning electron microscope (SEM) study of representative samples of enriched sulfides from major Cu deposits in northern Chile that suggest that supergene enrichment, like sulfide oxidation, is a bacterially mediated process. Bacteria were shown recently to nucleate placer Au formation (*6*).

Northern Chile–southern Peru is the world's premier Cu province and contains at least 12 major porphyry-type Cu deposits that display well-developed zones of supergene enrichment (*7*); ten of them are or have been exploited and the other two will be soon. The enrichment zones, ranging from 50 to 300 m thick (Fig. 1), were generated cumulatively as ground-water tables descended (*2*, *7*) under semiarid climatic conditions during the mid-Tertiary.

Representative samples of supergene enriched Cu ores were collected from high-grade veins in three of the major porphyry-type deposits mined in northern Chile: Chuquicamata (*8*) (Fig. 1), Quebrada Blanca (*9*), and El Salvador (*10*). The samples, from the uppermost 40 m of the respective enrichment zones, contain mas-

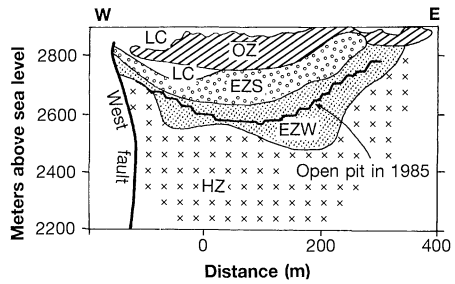

Fig. 1. Representative section of the Chuquicamata porphyry Cu deposit (*8*), northern Chile, that shows the position of supergene enrichment. Symbols: LC, leached capping, which was depleted of Cu by downward-migrating solutions; OZ, oxidized zone, where Cu was partially fixed as oxidized minerals, separated by a paleoground-water table from the enrichment zone (EZS, strong enrichment zone; EZW, weak enrichment zone); and HZ, hypogene zone, containing chalcopyrite, pyrite, and other sulfide minerals.

R. H. Sillitoe, 27 West Hill Park, Highgate Village, London N6 6ND, UK.
R. L. Folk, Department of Geological Sciences, University of Texas, Austin, TX 78712, USA.
N. Saric, Sociedad Minera Pudahuel S. A., Avenida Ricardo Lyon 527, Santiago, Chile.
*To whom correspondence should be addressed.

sive, steely chalcocite-group minerals, which are the hallmark of mature enrichment zones. Only small amounts of chalcopyrite and pyrite are present as unreplaced remnants in the chalcocite-group minerals. The samples contain >50% Cu by weight. The samples represent the latest stage of the mid-Tertiary enrichment process, which, because of its cumulative nature, destroyed the physical evidence for the earlier stages (3).

Freshly broken pieces of the samples were etched for 30 min with 10% HCl; this treatment readily dissolves chalcocite-group minerals but leaves other sulfides. We did not saw or polish the samples, as this may induce the formation of confusing artifacts. After etching, the samples were mounted immediately on Al stubs and then were spray-coated with Au for 40 s. The rapidity of the treatment precluded contamination by modern living bacteria.

Nannobacteria are spherical to bean-shaped objects with typical diameters of 0.05 to 0.2 μm. To identify them positively, one must use a SEM with a capability of high resolution to >×50,000, although most nannobacteria become visible at ×20,000. For overall scanning, we used chips with an area of 1 cm^2. For quantitative counting, we crushed and sieved the chips into 0.25- to 0.5-mm particles. Grains and fields were selected randomly at ×1000, then magnification was increased to ×20,000 and the small Energy Dispersive System screen was used, which covers an area of 2 μm by 2 μm at this magnification.

SEM examination revealed the presence of abundant bacterioform bodies ranging in shape from spherical to beanlike and in size from 0.03 to 0.2 μm. They are interpreted as fossilized dwarf forms of bacteria or nannobacteria (*11, 12*). Nannobacteria are defined on the basis of morphology, and we are awaiting confirmation of their biologic origin. The nannobacteria occur in clusters, just as modern bacteria do, because they flock to food and multiply geometrically; adjoining areas are deserted. In single chalcocite crystal faces, we found that some layers of the mineral were packed solidly with nannobacteria 0.03 to 0.05 μm in size, whereas others had no nannobacteria (Fig. 2A). Other samples showed areas of massive chalcocite that appeared to be composed entirely of nannobacteria (densities ~1000 per 4 μm^2), whereas 2-μm polyhedral crystals immediately adjacent had none. The two domains may represent different minerals of the chalcocite group. Our data show that bacteria are clustered closely along the replacement fronts between chalcopyrite or pyrite and chalcocite and are scarce in areas of chalcocite more than 2 mm from chalcopyrite or pyrite (Fig. 2B; Table 1). Nannobacteria appear to have bored into chalcopyrite or pyrite, and removal of the original chalcocite by etching revealed along the contact a coat of nannobacteria 0.1 to 0.2 μm across (Fig. 2C). The bacterioform texture may have been eliminated by progressive recrystallization of chalcocite away from the replacement fronts. Remnant biomass was not detectable in the chalcocite samples, so our identification of nannobacteria is based on the similarity of the sizes, shapes, and clustering patterns to those of nannobacteria in carbonate rocks (*11*). Because of the small size of the nannobacteria, we were unable to determine the mineralogy of specific individuals with the SEM. Presumably the nannobacteria protrude when etched because they are surrounded by C films representing the original cell walls.

Bacteria, especially members of the genus *Bacillus*, can concentrate a variety of metals on their anionic cell walls or, occasionally, within themselves (*5, 13*). This process of biosorption has commercial applications, including the treatment of acid drainage from abandoned Cu mines (*14*). Copper ions supplied in various forms, including sulfate solutions comparable to

Table 1. Nannobacteria per 4-μm^2 area of chalcocite. Nannobacteria are most abundant in samples containing remnant grains of chalcopyrite or pyrite.

Number of nannobacteria	Number of 4-μm^2 areas counted			
	1-cm^2 piece of chalcocite, Chuquicamata	Crushed chalcocite, El Salvador	Crushed chalcocite, Chuquicamata	Crushed chalcocite + chalcopyrite-pyrite, Chuquicamata
0	23	25	20	14
1 to 3	15	5	4	5
4 to 10	5	3	0	1
11 to 31	4	6	1	0
32 to 100	3	1	0	1
100 to 310	0	0	0	2
310 to 1000	0	0	0	2

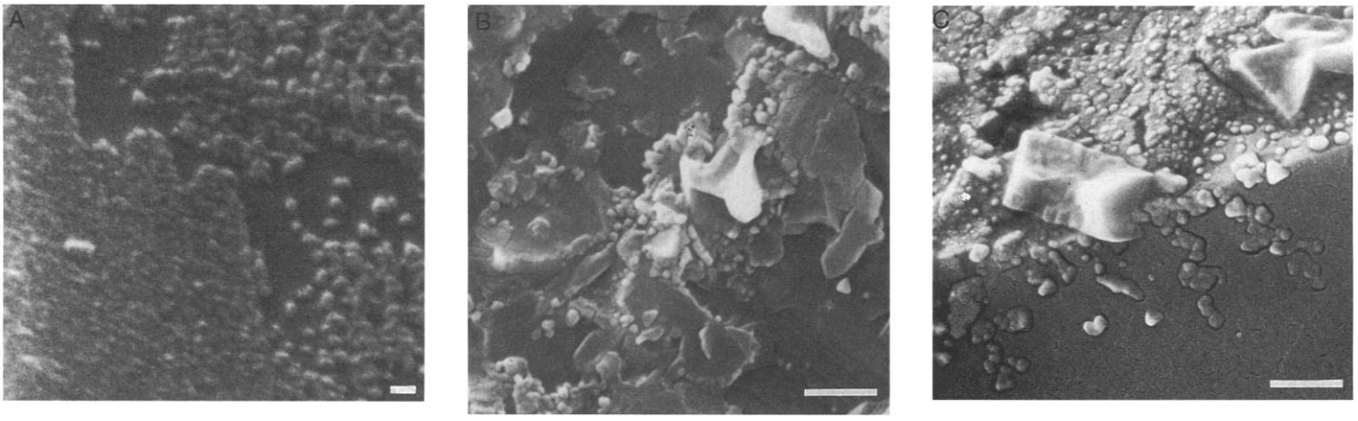

Fig. 2. SEM micrographs of etched supergene chalcocite-group minerals. (**A**) The top sheet of the mineral appears to be composed almost entirely of 0.03- to 0.05-μm nannobacteria, closely packed at left and widely dispersed at right. The underlying surface shows no evidence of nannobacteria (×50,000). Scale bar, 0.1 μm. (**B**) Chalcopyrite-pyrite remnants protrude and are under attack by bean-shaped nannobacteria (×15,000). Scale bar, 1 μm. (**C**) Replacement front between chalcocite and chalcopyrite-pyrite, with all the former etched away. The top surface, covered with scattered nannobacteria, was the original boundary between chalcocite and chalcopyrite-pyrite; the vertical surface represented by the darker, lower part of the micrograph is a fresh break. Nannobacteria appear to have bored into the chalcopyrite-pyrite (×15,000). Scale bar, 1 μm.

those responsible for supergene enrichment, may bind to cell walls in large quantities (*15*). Therefore, the collection and concentration of Cu ions seem to have been the most likely function of these putative bacteria in the enrichment process. However, the electron transfer involved in chalcocite enrichment (*16*) also may be catalyzed bacterially (5). Data on S isotopes (*17*) and theoretical modeling (*18*) show that the S in supergene chalcocite is inherited from the hypogene sulfides that it replaced. Hence, the bacteria cannot be of the type dedicated to the reduction of sulfate ions (in the descending solutions) to sulfide. Microbial fixation of Cu at active replacement fronts between hypogene sulfides and chalcocite may be a critical kinetic factor in the enrichment process.

Consequently, climatic or hydrologic conditions that favor the proliferation of bacteria may be an important control on the rate and efficiency of supergene enrichment. Indeed, the hyperarid conditions responsible for the mid-Miocene cessation of enrichment in northern Chile–southern Peru (*7*, *19*) may have been inimical to the bacterial activity. Most of the enrichment in northern Chile–southern Peru took place 100 to 300 m beneath the paleosurface (Fig. 1), which is shallow relative to the maximum recorded depth of ~4 km for subterranean microbial activity (*20*).

REFERENCES AND NOTES

1. W. H. Emmons, *The Enrichment of Ore Deposits (U.S. Geol. Surv. Bull. 625*, Government Printing Office, Washington, DC, 1917); A. Locke, *Leached Outcrops as Guides to Copper Ore* (Williams and Wilkins, Baltimore, MD, 1926).
2. G. H. Brimhall, C. N. Alpers, A. B. Cunningham, *Econ. Geol.* **80**, 1227 (1985).
3. C. N. Alpers and G. H. Brimhall, *ibid.* **84**, 229 (1989).
4. L. E. Murr, *Miner. Sci. Eng.* **12**, 121 (1980); B. J. Ralph, in *Comprehensive Biotechnology*, C. W. Robinson and J. A. Howell, Eds. (Pergamon, Oxford, 1985), vol. 4, pp. 201–234; S. Bustos, S. Castro, R. Montealegre, *FEMS Microbiol. Rev.* **11**, 231 (1993); R. Montealegre *et al.*, in *Biohydrometallurgical Technologies*, A. E. Torma, J. E. Wey, V. L. Lakshmanan, Eds. (Minerals, Metals, and Materials Society, American Institute of Mining Engineers, New York, 1993), pp. 1–14.
5. M. N. Hughes and R. K. Poole, *Metals and Microorganisms* (Chapman & Hall, London, 1989).
6. J. R. Watterson, *Geology* **20**, 315 (1992); G. Southam and T. J. Beveridge, *Geochim. Cosmochim. Acta* **58**, 4527 (1994). These are morphologic and experimental studies, respectively.
7. R. H. Sillitoe, in *Geology of the Andes and Its Relation to Hydrocarbon and Mineral Resources*, G. E. Ericksen, M. T. Cañas Pinochet, J. A. Reinemund, Eds. (*Earth Science Series Volume 11*, Circum-Pacific Council for Energy and Mineral Resources, Houston, TX, 1990), pp. 285–311.
8. R. Flores V., in *Actas 4th Congreso Geologico Chileno* (Universidad del Norte, Antofagasta, Chile, 1985), vol. 2, pp. 228–249.
9. J. P. Hunt, J. A. Bratt, J. C. Marquardt L., *Min. Eng.* **35**, 636 (1983).
10. L. B. Gustafson and J. P. Hunt, *Econ. Geol.* **70**, 857 (1975).
11. R. L. Folk, *J. Sediment. Petrol.* **63**, 990 (1993).
12. ———, *Géogr. Phys. Quat.* **48**, 233 (1994).
13. T. J. Beveridge and W. S. Fyfe, *Can. J. Earth Sci.* **22**, 1893 (1985); M. D. Mullen *et al.*, *Appl. Environ. Microbiol.* **55**, 3143 (1989); R. J. C. McLean and T. J. Beveridge, in *Microbial Mineral Recovery*, H. L. Ehrlich and C. L. Brierley, Eds. (McGraw-Hill, New York, 1990), pp. 185–222.
14. C. L. Brierley, in *Microbial Mineral Recovery*, H. L. Ehrlich and C. L. Brierley, Eds. (McGraw-Hill, New York, 1990), pp. 303–323.
15. T. J. Beveridge and R. G. E. Murray, *J. Bacteriol.* **127**, 1502 (1976); N. H. Mendelson, *Science* **258**, 1633 (1992).
16. R. L. Andrew, *Miner. Sci. Eng.* **12**, 193 (1980).
17. C. W. Field and L. B. Gustafson, *Econ. Geol.* **71**, 1533 (1976).
18. J. Ague and G. H. Brimhall, *ibid.* **84**, 506 (1989).
19. R. H. Sillitoe, C. Mortimer, A. H. Clark, *Trans. Inst. Min. Metall. B* **77**, 166 (1968); C. N. Alpers and G. H. Brimhall, *Geol. Soc. Am. Bull.* **100**, 1640 (1988); A. H. Clark, R. M. Tosdal, E. Farrar, A. Plazolles V., *Econ. Geol.* **85**, 1604 (1990).
20. K. Pedersen, *Earth-Sci. Rev.* **34**, 243 (1993).

21. Sample collection at Chuquicamata and El Salvador was carried out with the assistance and permission of Codelco-Chile. We thank W. S. Fyfe and J. R. Kyle for manuscript reviews and R. Espejo for discussions.

19 February 1996; accepted 20 March 1996

Oceanic Anoxia and the End Permian Mass Extinction

Paul B. Wignall and Richard J. Twitchett

Data on rocks from Spitsbergen and the equatorial sections of Italy and Slovenia indicate that the world's oceans became anoxic at both low and high paleolatitudes in the Late Permian. Such conditions may have been responsible for the mass extinction at this time. This event affected a wide range of shelf depths and extended into shallow water well above the storm wave base.

The mass extinction at the end of the Permian marks a serious biotic crisis: both the marine and terrestrial biota suffered near annihilation (*1*). The timing and causes of this event have been uncertain: Sequence stratigraphic analysis of numerous sections have shown that the Permian-Triassic (P-Tr) boundary straddles an interval of rapid, global sea-level rise (*2*, *3*). Similarly, an image of a protracted crisis spread over the last few million years of the Permian has been challenged; it may be a considerably more complex event involving an initial extinction separated by a period of radiation in the latest Permian before the wholesale slaughter at the end of the Permian (*4*). The final crisis may have been entirely restricted to the final one million years of the Permian.

The mechanism of the extinction has been much debated. The rapid eruption of the vast Siberian flood basalts was contemporary with the extinction, and the two events have been linked in several ways (5). Many boundary sections contain oxygen-restricted facies, which raises the possibility that marine organisms were killed by anoxia (*2*, 6). In this report, we demonstrate that anoxia occurred in much shallower water than previously recognized and show that sections of the high-latitude Boreal oceans were also affected by the anoxic event.

If anoxic-dysoxic conditions were responsible for the extinction, then several factors need to be demonstrated. (i) The conditions must have been sufficiently widespread (6). Most of the evidence for anoxia has come from equatorial and mid-southern paleolatitudes of the Tethyan Ocean. The nature of environmental changes in the high northerly paleolatitudes of the Boreal Ocean has been unclear. (ii) Anoxia must have affected areas of unusually shallow water, the repository for most marine invertebrate diversity. (iii) There must be a propinquitious relation in space and time between extinction and anoxia.

To answer these questions, we conducted a sedimentological and ichnological study of P-Tr boundary sections in Spitsbergen that lay on the margin of the Boreal Ocean and a similar study, combined with geochemical analysis, of the shallow-water, equatorial sections of western Tethys (northern Italy, southern Austria and Slovenia).

The P-Tr boundary in Spitsbergen has traditionally been placed at the contact between the Permian Kapp Starostin Formation, a cherty limestone and shale, and the shale and sandstone of the Vardebukta Formation (Griesbachian and Dienerian stages of the lowermost Triassic). Available biostratigraphic data are poor, and for the Kapp Starostin Formation, the carbon isotope stratigraphy revealed by its constituent brachiopod and coral fauna is the best guide to its latest Permian (Changxingian Stage) age (7). The Vardebukta Formation contains sporadic examples of the ammonoid *Otoceras boreale* near its base, and these are joined by the typical Triassic taxa *Ophiceras* and *Claraia* 20 to 30 m above the base (8). Defining the position of the base of the Triassic is a

Department of Earth Sciences, University of Leeds, Leeds LS2 9JT, UK.